FRP strengthening of web panels of steel plate girders against shear buckling. Part-II

FRP Strengthening of Web Panels of Steel Plate Girders against Shear Buckling
Part-II: Fatigue Study and Cyclic Series of Tests

Zaid Al-Azzawi[1], Tim Stratford[2], Michael Rotter[2], Luke Bisby[2]

[1] College of Engineering, University of Anbar
P.O. Box 55/ Ramadi (55431/Baghdad)- Anbar- IRAQ.

[2] School of Engineering, The University of Edinburgh.
AGB Building, The King's Buildings, Mayfield Road, Edinburgh, EH9 3JL, UK.

Corresponding author: Zaid Al-Azzawi
Email: zaidkani@yahoo.com – zaid.kani@uoanbar.edu.iq

ABSTRACT

The result of an experimental programme investigating a novel technique to strengthen web plates of steel plate girders against breathing fatigue due to shear buckling deformations is presented. An experimental test series is present in which six specimens were manufactured to simulate the end panel of a plate girder; these were strengthened with an optimized FRP retrofit panel that was developed in an earlier phase of the research project, and tested for plate girder web shear buckling deformation mitigation under repeated cyclic loading, as well as ultimate load capacity enhancement. Test results and non-linear finite element modelling demonstrated the efficiency of this technique for stiffening the web against these deformation and thus reducing the critical stresses, consequently increasing the fatigue life of the girders by a factor ranging between three and seven, depending on the applied stress range and the fatigue resistance assessment method. The research demonstrates the applicability of this novel FRP strengthening technique to prolong and extend the fatigue life of existing plate girder bridges.

Keywords: Steel bridges; Plate girders; Steel plates; FRP; Strengthening; Fatigue; Buckling; Shear.

INTRODUCTION

The issue of damaged, deteriorating, or deficient bridges is a topic of considerable importance in the developed (and developing) world. Steel and composite steel-concrete bridges constitute a large number of the existing bridges worldwide. With the increasing number of structurally deficient bridges in the world, there is a need to adopt durable materials and cost-effective strengthening techniques (Assoodani, 2014). This paper focuses on a novel strengthening technique using fibre reinforced polymers (FRPs) to address a specific deficiency in steel plate girder bridges related to shear buckling deformations of their web plates; the work seeks to stiffen, strengthen, and extend the fatigue life of such girders.

In the practical range of typical plate girder spans, shear stresses in the girders' webs are relatively low compared to the bending stresses in the flanges. As a result, the web plates in such girders are generally made from much thinner plates than the flanges. These web panels are consequently prone to instabilities (buckling) at relatively low shear forces. For structures with dominant cyclic loading, this can lead to the so called 'breathing' phenomenon, which is the case with repeated axle loading of plate girders in bridges. 'Breathing' is an out-of plane displacement of the web plates, under shear loading, which can induce high secondary bending stresses at the welded plate boundaries. Fatigue damage due to repeated cycles of these bending stresses at the plate boundaries is a particular concern for many such bridges.

Different techniques exist for strengthening steel structures; all of which have advantages and drawbacks. For instance, conventional techniques for strengthening steel structures – such as welding additional transverse/longitudinal stiffeners for example – require heavy equipment during installation, have fatigue performance concerns due to weld fatigue, and may result in a need for ongoing maintenance due to corrosion attack, etc. Amongst the available strengthening techniques and materials, the potential use FRPs is particularly appealing because of FRPs' resistance to corrosion, speed of installation, low weight, and high tensile strength-to-weight ratio.

A novel preformed corrugated FRP panel is introduced herein, which can be adhesively bonded to a plate girder web panel. The specific shape and configuration of the FRP panel was previously optimized using extensive finite element modelling that sought to minimize the cost of the FRP material and the quantity of adhesive used; taking the complexity of the multi-axial stress state in the web steel plate into consideration (Al-Azzawi et al., 2016). Tests were previously performed to verify the effectiveness of the FRP panels at increasing the shear buckling strength of web plates in steel plate girders, in addition to enhancing their fatigue performance, and also giving priority to maintaining the typical ductile failure associated with steel plate girders at the ultimate condition, since this is an important factor sometimes ignored by other common strengthening techniques. Fig.1 shows a typical steel plate girder with the proposed shear strengthening technique, in comparison to the more common flexural strengthening technique.

BACKGROUND

Research was undertaken at Lehigh University in the 1960s to study the fatigue behaviour of thin-web, welded plate girders (Yen and Mueller 1966). It was demonstrated that secondary bending stresses in the webs were caused by lateral (i.e. out-of-plane buckling) web deflections under cyclic loading. The magnitude of the deformations and the resulting stresses was as high as the yield strength of the web plate in some cases, leading to the development of fatigue cracks at the plate boundaries. The initial locations of fatigue cracks along the flanges adjacent to the web were shown to be in the regions of the highest secondary bending stresses, and comparing these stresses with the number of cycles at crack initiation, a clear correlation was observed (Yen and Mueller, 1966).

Roberts et al. (1995a) performed research studying the rate of fatigue crack propagation and fatigue limit loads for slender steel web plates subjected to cyclic shear loading. Similar observations to Yen and Mueller (1966) were made, however in this case the experimental

results were presented together with a theoretical procedure for predicting the residual shear strength of fatigue-cracked web panels. Roberts et al. (1995a) noticed that during fatigue tests the girders exhibited considerable web plate breathing, with pronounced shear buckles forming and reforming along the tension diagonals of the web panels during cyclic loading. Fatigue cracks formed along the toes of the welds between the web and boundary members, in regions of high secondary bending stresses caused by out-of-plane (i.e. buckling) deformations. The number of load cycles before fatigue crack initiation varied considerably; for higher load ranges the rate of propagation of fatigue cracks was reasonably uniform, whereas for lower load ranges it was variable.

On the basis of their research, Roberts et al. (1995b) stated that stress ranges at potential fatigue crack locations could be predicted using either nonlinear finite element analysis (FEA) or approximate analytical solutions. They also demonstrated that the fatigue assessment procedures recommended in the Eurocodes, based on either principal stress ranges or normal and shear stress ranges, provided conservative estimates of the fatigue life for slender webs subjected to web plate breathing under cyclic shear loading.

Skaloud and Zornerova (2005) also studied the fatigue response of slender plates in shear. They studied the limit state for the webs of steel plate girders subjected to repeated loading, and noted, unsurprisingly, that the response is affected by the cumulative damage process generated in the web under repeated loading.

A limited numbers of researchers have studied the use of FRP materials for strengthening the webs of steel plate girders under short term shear loading. One such study was by Okeil et. al. (2009), who investigated the use of externally bonded GFRP pultruded sections for this type of application. The pultruded GFRP sections in this study were bonded to thin-walled steel plates in orientations that were assumed to best contribute to the out-of-plane stiffness of the plate, rather than its in-plane strength, as is the more common practice in FRP strengthening applications. Beam (shear) specimens were tested to explore the out-of-

plane strengthening technique, increasing the ultimate capacity of the strengthened specimens by 56%; however reducing their ductility by a factor of four.

Miyashita et al. (2012) have presented a series of shear buckling tests on seven steel plate girders with carbon FRP (CFRP) sheets bonded to both sides of the web panels as substitutes for steel web plate material lost due to corrosion attack. Test variables included the web aspect ratio (a_w/d =1 and 1.5) and the plate slenderness ratio (h_w/t_w = 133 and 166). Different numbers of CFRP layers and carbon fibre orientations were used. Increases in the ultimate capacity of the specimens, between 6.2% and 29%, were reported, along with a proposed modification to Basler's equation (Basler, 1961) to account for the addition of bonded CFRP, showing a good correlation with their experimental results.

More recently, Assoodani (2014) conducted an experimental programme to study steel plate girders and steel-concrete composite plate girders retrofitted with CFRP composites adhesively bonded to the web plates and loaded primarily in shear. A combination of pultruded CFRP plates and fabric CFRP sheets was used in this case. The maximum increase in the capacity of the strengthened specimens was 132% for a specimen strengthened with mechanically anchored pultruded CFRP plates on both the tension and compression web plate diagonals.

Much of the available work on the use of FRP materials for strengthening plate girders against web plate buckling under shear loading has focused on application of existing FRP materials and products for such strengthening applications. Little work has been undertaken to develop custom FRP strengthening materials for such applications, and no research appears to be available in the literature addressing the performance of FRP strengthening systems for web plate buckling in steel plate girders under cyclic loads; in these applications both the stiffening of the web against out of plane 'breathing' deformations *and* the strengthening effect of the externally-bonded FRP on the ultimate limit state are relevant. Both of these issues are addressed in the current study.

EXPERIMENTAL PROGRAMME

Six specimens were manufactured to simulate the end panel of a plate girder and were strengthened with an optimized FRP retrofit panel that was developed in an earlier phase of the research project. These were subsequently tested for plate girder web shear buckling deformation mitigation under repeated cyclic loading, as well as ultimate load capacity enhancement.

Specimen Description

The tested specimens represent end panels of longer plate girders that would be made from several panels. The objective was to consider a web panel with low bending stresses but where high shearing forces exist, since such panels are most likely to suffer fatigue failure due to out-of-plane 'breathing' deformations. Instead of joining two end panels and testing them under a central point load, as is common in typical laboratory-scale testing of plate girder panels under shear loading, symmetry was exploited and only one panel was tested at any given time, as shown in Fig. (1). The specimens were provided with rigid-end posts to insure that the tension field was fully developed within the web plate. The web plate aspect ratio (a_w/h_w) was chosen as equal to 1.5, which is a common value assumed in design practice (Assoodani, 2014), and the web plate thickness was chosen (essentially arbitrarily, but informed by a range of testing considerations) as 2 mm. This resulted in a relatively high web plate slenderness ratio (h_w/t_w) of 245, where a_w, h_w and t_w are the length, height, and thickness of the web, respectively. This high slenderness ratio was chosen intentionally to best demonstrate the potential stiffening effect of the proposed FRP strengthening technique. The web plate was made from S275 grade steel (i.e. 275MPa nominal yield strength), while the flanges and stiffeners were made from S355 steel. The web and flange plates were welded together using a manual arc welder with a continuous all-round (5 mm) fillet weld. Fig. (2-a) shows a schematic of the test specimens used.

The preformed corrugated FRP panel section used in the current study and shown in Fig. (2-b) was made from three layers of either GFRP or CFRP using a vacuum bagged wet-layup process, and their resulting mechanical properties were determined experimentally. The GFRP laminate had a thickness of 1.43 mm and a modulus of elasticity (E_f) of 18.02GPa, while the CFRP laminate had a thickness of 1.67 mm and a modulus of elasticity of 48.12GPa; more details can be found in (Al-Azzawi et. al, 2018). The reason for changing the FRP section with respect to SP-6 (Fig. 2-b) is the different length of the FRP panel resulting from different alignment schemes as will be seen in the experimental programme.

Test Variables

The variables investigated in the cyclic loading test series presented herein are mainly the FRP material type and the alignment of the FRP stiffening/strengthening panels with respect to the compression diagonal; these are detailed in Table 1, which provides an overview of the experimental programme and the various specimens tested and parameters varied. The programme involves testing six plate girder sections. The first three specimens were (SP-1) the control specimen, (SP-2) a GFRP strengthened specimen, and (SP-3) a CFRP strengthened specimen. Specimens SP-2 and SP-3 were strengthened with diagonal FRP panels (oriented at an angle of 34° from horizontal) and tested for shear buckling under low cycle static load, to failure, as a precursor to the subsequent three tests on strengthened specimens under cyclic loads. The cyclic tests involved testing three additional specimens; two of these were GFRP (SP-4) and CFRP (SP-5) strengthened specimens that were identical to the static specimens SP-2 and SP-3, respectively. A third cyclic loaded specimen (SP-6) was also tested, for which the alignment of the CFRP strengthening system was changed to 45° from horizontal, rather than 34°, to assess its effects on the efficiency of the proposed strengthening technique. Both alignments are illustrated in Fig. (3), which gives photographs of specimens strengthened with CFRP after the FRP materials were bonded.

Specimen Preparation

Before FRP bonding the specimens were grit-blasted to the required surface roughness to ensure a high quality bond with the epoxy adhesive used. The specimens were then cleaned until a surface free from dust and debris was reached, and then washed with acetone to insure that the surface was free from contamination and oxidation products. Sikadur 330 epoxy was then applied to the steel plate, and the FRP panel was adhered. The FRP panel was then attached to the specimen using a special fixture to hold it in position. Finally, a uniformly distributed load was applied to press the panel toward the steel plate to reduce air bubbles. This load was maintained for 24 hours until the initial set of the epoxy adhesive, and then removed.

Test Instrumentation

Fig. (4) shows the instrumentation used in the tests, including diagrams and photos for both the statically and cyclically loaded specimens. The first three specimens had four single bonded foil strain gauges (S7-S10) attached to their top and bottom flanges. A single strain gauge rosette was used in the centre of the web plate to measure the vertical, horizontal, and diagonal strains. The location of the LPs and strain gauges are shown in Fig. (4-a) where S refers to strain gauges and LP refers to linear potentiometers. Five of the LPs (LP1 to LP5) were used to determine the out-of-plane displacements of the web plate, two LPs (LP6 and LP7) were used to monitor the potential rigid-body rotation in the testing rig (i.e. out-of-plane movement), one LP (LP-8) was used to determine the deflection at the bottom end of the tested plate under the applied load, and a final two LPs (LP9 and LP10) measured the in-plane rotations in the columns of the restraining frame used to test the samples.

To reduce the number of channels and the large amount of data produced during the cyclic loading tests, a number of changes were made to the instrumentation as the testing programme progressed; these are highlighted in Fig. (4-b) and Fig. (4-c). For the three cyclic

tests only LP-2, LP-9, and LP-10 were maintained in position, to measure the central out-of-plane displacement and the in-plane rotations of the tested specimen. LP-1 was moved to a new position (shown in Fig. 4-b) because this location displayed large out-of-plane displacements, comparable or even some times exceeding the central out-of-plane displacement, during the initial static testing.

The bonded foil strain gauges were distributed within the tension field zone. In addition, a single rosette strain gauge was attached to both faces of the web plate at a distance of 112.5 mm from the plate tension corner where the maximum strain was anticipated using the finite element model (Al-Azzawi et al., 2016). In this way, the secondary bending stresses could be calculated and compared to those experienced in the unstrengthened control tests. For the final cyclic specimen, SP-6 (with CFRP strengthening at 45° inclination from horizontal), an attempt was made to compare the secondary bending strains between the estimated location and at the corner of the tension field by using 2 additional strain gauge rosettes on each face of the web plate. In addition, the tension field strains were measured at 45° (parallel to the expected tension field), as can be seen from Fig. (4-c).

Strain gauge and displacement gauge (LP) readings were recorded at a rate of 10 Hz using a Vishay 7000 data acquisition system. Loading was applied using a 1000kN servo-hydraulic Instron actuator, at a stroke rate of 1.0 mm/minute for the static tests and a loading frequency of 2.0Hz for the cyclic tests, with the specimens and actuator mounted within a steel self-reacting restraining frame. Before each test, the central out-of-flatness (initial imperfections) of the web plates was measured and recorded for further investigation with post testing numerical modelling.

Testing Method

For the first three pseudo-static tests, the load was applied through six cycles, with each cycle increasing the load by 20% of the ultimate capacity of the unstrengthened control specimen.

This was done to detect possible debonding of the FRP strengthening systems at different loading stages. In the final cycle, the load was increased continuously until the specimen failed.

For the cyclic (fatigue) tests, the loading range was chosen between 40-80% of the ultimate capacity of the corresponding pseudo-static testing control specimen. Each specimen was tested for two million load cycles, except SP-4, which was tested for only one million load cycles because it demonstrated only very limited breathing during testing. All tests were halted periodically to check the specimen and take the residual readings. After the prescribed number of loading cycles was completed, the specimen was tested again for its ultimate static shear strength using the same testing procedure as that used for the static tests.

EXPERIMENTAL RESULTS

Table 2 shows the experimental results both for the pseudo-static and cyclic tests. For each specimen the designation is given along with the measured initial imperfection, the test method applied, and the ultimate load. Details of the cyclic regime, including the number of cycles are also provided for the cyclic tests. It is noteworthy that, because no FRP debonding whatsoever was detected for any specimen at any loading stage, the residual ultimate loads of the cyclic tests are likely to be very close to their corresponding static ultimate strength, taking into consideration the difference in the behaviour resulting from different initial imperfections which are well known to play a major role in the behaviour of plate girders, especially strengthened ones as discussed in the following sections. It is also important to note that in Table 2 the designed loading range of 40-80% was not fulfilled exactly because the preliminary calculation are dependent on the pseudo-static test specimens (SP-2 and SP-3) while the final loading range calculations (which is simply the applied load divided by the ultimate load capacity) is performed based on the final residual ultimate capacity of cyclic

specimens (SP-4, SP-5 and SP-6). This what caused the variations between the designed and the applied loading ranges.

Fig. (5-a) compares the load versus central out-of-plane displacement (to be called buckling curves from now on) for all tested specimens. Generally, it can be seen that SP-6 (CFRP-45°) performed the best among all specimens and increased the ultimate shear strength by 88%. Most of the buckling curves followed the same pattern where there behaviour was linear up to approximately 80% of the ultimate capacity and then curved dramatically towards the failure plateau forming a bilinear pattern. However, the only exceptions to this general behaviour were (SP-3 and SP-4) because their buckling mode followed their reversed initial imperfection. This caused some reduction in their strengthening effect but it did not reduce the stiffening effect within the working stress limits. At this point it should be mentioned that in spite of the fact that the proposed strengthening technique is designed to be mostly effective when the buckling mode is toward the bonded FRP section (induced by the pre-buckling mode caused by the unbalanced composite section), but even if the buckling direction is reversed due to the reversed initial imperfection (SP-3 and SP4) this does not suggest that the strengthening technique will lose all its efficiency because as can be seen from Fig. (5-a) They still perform better than the control specimen, especially within the working stress limit which is usually not exceeded in practical cyclic loading. Nevertheless, it is preferable to investigate the direction of the initial imperfection before tending to bond the new FRP section on either of the steel plate faces to get most possible strengthening efficiency.

Fig. (5-b) shows the variation of the maximum out-of-plane displacement with the applied loading cycles. From this figure it can be seen that the out-of-plane displacement was almost constant all over the 2 million cycles of loads except when the loading amplitude was changed for practical considerations as marked on the figure. This is a good indication that no debonding took place during the cyclic test and this conclusion was further confirmed by

visual observation during and after the tests. However, by looking at Fig. (5-b) it is worth mentioning that SP-6 had lesser out-of-plane displacement than SP-5 (both having CFRP) because the 45° strengthening technique was much more efficient than the diagonal one with much higher stiffness. But, SP-4 (GFRP) had smaller out-of-plane displacement because of the reversed buckling mode.

Assessing the Stiffening Effect of the Proposed Strengthening Technique

Fig. (6-a) shows the dimensionless version of the buckling curves. The load was simply made dimensionless by dividing it by the corresponding shear yielding load using the Von Mises criterion where the yielding shear stress can be taken equal to ($f_y/\sqrt{3}$). For the displacement axis, this was performed by dividing the out-of-plane displacement by a limiting displacement (the limit where the behaviour of the curves turns into non-linear).

The stiffening effect was quantified by dividing the area between the y-axis and the buckling curve of the control specimen by the corresponding area of each of the strengthened specimens except the ones who had a reversed buckling mode (SP-3 and SP-4). This is called the stiffness index and is illustrated in Figs. (6-b) and (6.c) and shown in Table 3, for more details about this index refer to (Al-Azzawi et al., 2018). It is worth mentioning that in order to be able to fairly compare the stiffness of the strengthened specimens with the unstrengthened control specimen (SP-1), the initial imperfection needs to be compatible which is experimentally very difficult because each specimen had different initial imperfection. This problem was solved by creating a new control buckling curve for each different initial imperfection using finite element analysis, see Fig. (6-e). The model was verified against experimental data as will be seen in the numerical modelling section and showed very good convergence. Hence, the difference in the initial imperfection was taken into consideration in the calculations of the stiffness indicators.

However, From Table 3 it can be seen that the proposed strengthening technique succeeded in increasing the stiffness indicator of the specimens by a factor ranging between 3 to 9 times the stiffness of the corresponding control ones.

This high increase in the stiffness of the strengthened specimens was not on the expense of ductility. As a matter of fact the energy absorption capacities of the strengthened specimens were even increased by a factor ranging between 1.5 and 2.5 that of the control specimen as can be seen in Table 3. This increase in the absorption capacity was calculated by dividing the area between the x-axis and the buckling curve for the strengthened specimen by the corresponding are of the control one. This is called the energy absorption index and can be seen in Figs. (6-b) and (6-d), for more details about this index refer to (Al-Azzawi et al., 2018). SP-6 (CFRP-45°) succeeded the best in both the stiffness and energy absorption criteria. However, it is very important to note that Fig. (5-a) might imply that the proposed strengthening technique reduced the ductility, but actually it did not. This is because the unloading part of the curve for each specimen does not mean failure. Apart from SP-2 (GFRP) the specimens never reached a failure plateau and there was no drop in the ultimate load capacity, on the contrary there was still a possibility for specimens to undergo extra loading but the test was stopped manually either because the load reached a high level that may lead to the distortion of the testing rig (SP-6 for instance) or because the deformation was too high (SP-1). It is believed that the tests could have been continued to higher deformational levels just like the control specimen (SP-1). This is why the strengthened specimens curves where extended almost horizontally following the trend of the curve itself to the same deformation level as the control one as can be seen in Fig. (6-a). The above-mentioned ductility calculations were based on the extended curves shown in Figs. (6-a and 6-d) rather than Fig. (5-a).

Fatigue Performance of the Strengthened Specimens

There are several methods available to estimate the fatigue life expectancy for different members and mechanical systems depending on their function, material, and the type of applied loads. However, for structural members undergoing high-cycle fatigue (members that do not encounter high plastic strain within their working stress limits), the stress range method is globally accepted and adopted in most international standards like AASHTO, AISC, and the Eurocode.

For unclassified details, Eurocode 3 recommends that the fatigue assessment be based on the geometric stress range. This is defined as the maximum principal stress range in the vicinity of a weld (Robert et. al., 1995). In the current study the values of the principal surface stress ranges calculated from the experimental strain measurements for the cyclic strengthened specimens (SP-4, SP-5, and CP-6) at the diagonal tension corner near the welding and the ones determined using finite element analysis for the unstrengthened control specimen will be used in conjunction with the Eurocode fatigue strength curves to estimate the life expectancy of the specimens and study the effect of the proposed strengthening technique in reducing the stress ranges for the same service loads, and consequently to increase their fatigue life limit. Taking the maximum experimentally measured surface stress range at the corner for each of the cyclically tested strengthened specimens (SP-4, SP-5, and SP-6) and comparing it with the corresponding stress range associated with the control specimen for the same applied load range. In this comparison, the applied load range was taken equal to 20-80% of the ultimate capacity of the control specimen (SP-1). It is worth mentioning at this point that apart from the un-strengthened control specimen (SP-1), the other two specimens tested under static loading (SP-2 and SP-3) are meant to demonstrate the increase in stiffness indices due to the proposed strengthening technique which then leads to a reduction in the deformation due to shear buckling which would ultimately cause fatigue failure. In addition to that, they acted as a precursor for the corresponding cyclic specimens (SP-4 and SP-6) to determine their

ultimate load capacity in order to be able to determine the possible loading ranges during the cyclic tests. SP-2 and SP-3 were not used for the fatigue calculations itself presented in this section.

Fig. (7) demonstrates how reducing the stress range is reflected by increasing the fatigue life expectancy represented by the number of the loading cycles (N) using the Eurocode fatigue curves for normal stress range ($\boldsymbol{\Delta\sigma_r}$) and shear stress range ($\boldsymbol{\Delta\tau_r}$) with a detail category of 125MPa and 80MPa, respectively. These stress ranges are the highest classification curves for a welded joint section. In this figure, the experimentally measured stress range is projected on the prescribed detail category taken from Eurocode 3 in comparison to the higher stress range of the control specimen under the same loading amplitude. This reduction in the stress ranges for the same loading amplitude results from strengthening the specimen with the proposed FRP corrugated panel designed and implemented in the current study. From Fig. (7), it can be seen that the shear stress range criterion gives a fatigue life expectancy several times higher than the corresponding normal stress range criterion. This high discrepancy between the two methods raises a lot of questions about the validity of the shear stress range as a criterion for the assessment of fatigue life expectancy; which is recommended solely by the Eurocode and non of the other standards use this method.

Tables 4 shows the calculations of the number of cycles required for the fatigue failure according to the Eurocode for the three strengthened specimens tested cyclically in this work. For the strengthened specimens, the strain values at the specific loading range were taken directly from the available test data and then transferred into stresses by multiplying them by the modulus of elasticity and then the maximum principal stress is calculated using Mohr circle. The same procedure was followed for the control specimen except that the strains at the corner were determined using the finite element model for the same loading range. In Table 4, ΔL is the applied load range, $\Delta\mathcal{E}$ is the measured normal strain range, $\Delta\sigma_r$ is the

calculated normal stress range, $\Delta\gamma$ is the measured shear strain, $\Delta\tau_r$ is the calculated shear stress range, $N_{\sigma r}$ is the number of cycles determined from the normal stress range criterion, and $N_{\tau r}$ is the number of cycles determined from the shear stress range criterion.

From Table 4, SP-6 (CFRP-45° strengthened specimen) offers the best enhancement in the fatigue life estimation with a factor of 3.8 times the control one, in comparison to 3.6 and 3.3 for SP-4 (GFRP strengthened) and SP-5 (CFRP-diagonally strengthened) specimens, respectively. However, this improvement in the fatigue life estimation is obviously restricted by the capacity of the control specimen and the applied loading ranges in addition to the yield stress limit of the web plate. The strain in the control specimen was several times higher than the yielding strain but the limit of yield stress (275MPa) governed the calculations. So, it is expected that the enhancement in the fatigue life estimations would be several times higher if a fatigue strain criterion were to be applied instead of the current stress criterion or a web steel plate with higher yield stress is used.

Finally, Fig. (8) shows the variations in the improvement of the fatigue life of the strengthened specimens with changing the loading range within the limit of the control specimen. In this figure, the resulting number of cycles is drawn as a function of the loading ranges both for the normal and shear stress criteria. From this figure, it can be seen that reducing the loading range from (ΔL=70kN) to (ΔL=50kN) results in moderate increase in number of loading cycles, however, reducing the stress range further will lead to a dramatic increase in the number of cycles until the limit of (ΔL=35kN) where the number of loading cycles is increased logarithmically reflecting an endurance limit.

NUMERICAL MODEL OF THE CONTROL SPECIMEN

Geometrical and material non-linear finite element analysis (GMNA) was used to model the control specimen. The web steel plate was modelled using a nine node reduced integration shell element S9R5, which has five degrees of freedom per node. S9R5 elements are meant

for slender plates and were derived originally according to Kirchhoff thin plate bending theory. This element is not available in *Abaqus* standard CAE and can be used only through an *Abaqus* input file. A Matlab code was written to create the nodes and element incidences to be incorporated in *Abaqus* input files. The size of the web elements was chosen to be 20×20 mm which satisfies the condition of (h_w/20) based on a full convergence study published in a previous paper (Al-Azzawi et al. 2015). The initial imperfection was found using the elastic Eigen buckling modes; these were initiated using the buckling analysis available in *Abaqus CAE* and then the experimentally measured initial imperfection were imposed using *Abaqus* script commands in the input file. All other parts of the specimen (flanges and stiffeners) were modelled using S4R shell element available in standard *Abaqus CAE*. The flanges and stiffeners elements size were approximately 20×20 mm and 10×10 mm, respectively. This size of elements was chosen based on their corresponding member size and according to a convergence study which showed that changing these element sizes does not cause any significant change in the numerical outcomes. Fig. (9) shows the finite element model for the control specimen and the corresponding contour distribution for the out-of-plane displacement.

An elastic-perfectly plastic stress-strain curve was adopted for the steel constitutive model, with a modulus of elasticity (E_s) of 200GPa and yield strength (f_y) of 275MPa and 355MPa for the 2 mm web plate and the flanges and stiffeners, respectively.

Fig. (10) compares the numerical model outputs against the experimentally measured out-of-plane displacement and in-plane deflection. The numerically predicted strain at the centre of the web plate is also verified against the experimental ones in Fig. (11) both for the front and back faces of the web steel plate. From both figures, it can be stated that the model is valid and capable of predicting both the strength and the deformational behaviour of the control specimen with high accuracy.

CONCLUSIONS

The current paper is part of an extensive experimental programme aiming to propose a new strengthening technique to stiffen thin-walled steel plate girders against shear buckling and breathing. In order to ensure the viability of this technique, certain criteria must be met. The proposed strengthening technique needs to be cost effective and easy to apply. It should also maintain the typical ductile failure associated with steel plate girders, something which is usually neglected in other common strengthening techniques. Additionally it should be possible to implement the solution on only one face of the plate girder to ensure applicability in cases where reaching the second face is difficult and/or costly. Provided all these conditions can be met the method will provide a relevant and practical solution with many advantages over the limited existing techniques.

In part-I of this paper (Al-Azzawi et. al, 2018), it has been shown that all of the goals highlighted above were achieved in the current study by proposing a new engineered preformed corrugated FRP strengthening panel. The FRP panel is bonded along the compression diagonal of the web plate in a 45° alignment scheme. The unique design of this new FRP panel enables effective stiffening of steel plate girder whilst also meeting the additional criteria outlined above. The proposed preformed corrugated FRP panel reduced the required FRP material by approximately 8 times (volumetrically) and the required epoxy bond surface area by 7 times. This leads to a reduction in the cost of the strengthening process whilst causing no reduction to bond strength of the specimen and maintaining the typical ductile failure associated with intact steel plate girders. The preservation of bond strength can be attributed to the design of the corrugated FRP panel where it is strong in the major axis along the compression diagonal and weak along the secondary axis along the tension diagonal to allow the steel plate to extend in tension without debonding.

The panel was designed to be applied to only one face of the web plate forming a prebuckling mode which forces the specimen to buckle towards the outermost fibres of the

FRP panel. This results in the FRP panel being stressed in tension, the stress state for which it performs most efficiently. The only drawback of single side application is that if the web plate has a reversed initial imperfection it could lead to a reversed buckling mode. In this case the outermost FRP fibres would be in compression instead of tension forming local wrinkles causing a premature failure of the FRP panel; however, this could only happen beyond the working stress limit. This problem can be solved by choosing the correct web face to bond the FRP panel by tracking the initial imperfection mode (which is believed to be difficult in field applications). In the latter case where it is difficult to track the initial imperfection, bonding the FRP panel to both sides of the web steel plate will be preferable. However, if this is not possible then the stiffening effect will remain the same and the fatigue performance will be enhanced as suggested. The only drawback would be that the ultimate strength will not be increased as expected, which is something unimportant unless part of the original design.

The FRP panel was optimized with respect to different variables that can affect its performance and its efficiency was tested both under static loading in part-I of this work and cyclic loading regime in the current work (part-II). From the results presented in this paper, it can be concluded that the proposed strengthening technique survived up to 2 million cycles of loading with no signs of debonding regardless the fact that the applied cyclic loading range was 40-80% of the ultimate static capacity for the strengthened specimens, which is considered higher than the practical loading range which usually does not exceed 60 to 70% of the ultimate capacity.

As a final statement, using the proposed strengthening technique minimizes the economic and temporal cost of strengthening, increases the life expectancy of the plate girder by up to 7.0 times that of the original design and increases its ultimate capacity by 88% whilst maintaining a ductile failure mode.

ACKNOWLEDGMENTS

This work was sponsored by the Ministry of Higher Education and Scientific Research in Iraq. The School of Engineering at the University of Edinburgh, which is part of the Edinburgh Research Partnership in Engineering (ERPE), is acknowledged for providing support to this project.

REFERENCES

Al-Azzawi, Z., Stratford, T., Rotter, M., and Bisby, L. (2015). “Effect of flange and stiffener rigidity on the boundary conditions and shear buckling stress of plate girders.” 16th European Bridge Conference, 23-25th June, Edinburgh, 12 pp.

Al-Azzawi, Z., Stratford, T., Rotter, M., and Bisby, L. (2016). “FRP Strengthening of Web Panels of Steel Plate Girders against Shear Buckling under Static and Cyclic Loading.” ACMBS MCAPC VII, 24-26 August 2016, Vancouver, British Columbia, Canada, 6 pp.

Zaid Al-Azzawi, Tim Stratford, Michael Rotter and Luke Bisby (2018). "FRP Strengthening of Web Panels of Steel Plate Girders against Shear Buckling Part-I: Static Series of Tests," Composite Structures, 206 (2018) 722-738.

American Association of State Highway Transportation Officials (1994). AASHTO LRFD Bridge Design Specifications, first edition, Washington D.C.

American Institute of Steel Construction (1994). Specification for Structural Steel Buildings, ANSI/AISC 360-10, 2010, Chicago, IL.

Assoodani, F. A. (2014). “Shear behaviour and strength of CFRP retrofitted steel plate girders and steel-concrete composite plate girders.” PhD thesis, University of Technology, Iraq, July 2014, 610 pp.

European Committee for Standardisation (ENV 2005). Eurocode 3: Design of Steel Structures- Part 1-9: Fatigue. EN 1993-1-9: 1993. Brussels: CEN.

Miyashita T., Okuyama Y., Nagai M., Wakabayashi D., Koide N., Hidekuma Y., Kobayashi A., Horimoto W. (2012). “Shear buckling tests of steel girder bonded carbon fiber reinforced plastic on its web.” Structural faults and repair, Edinburgh.

Okeil, A.M., Bingol, Y., and Ferdous, Md.R. (2009). “Novel technique for inhibiting buckling of thin-walled steel structures using pultruded glass FRP sections.” Journal of Composites for Construction, 13(6), 547-557.

Roberts, T. M., Davies, A. W., and Bennett, R. J. H. (1995b). “Fatigue shear strength of slender web plates.” Journal of Structural Engineering, October 1995, 1369-1401.

Roberts, T. M., Osman, M. H., Skaloud, M. and Zornerova, M. (1995a) “Fatigue crack propagation and residual strength of slender web panels.” International Colloquium on Stability of Steel Structures, Budapest.

Schnerch, D.A. (2005). “Strengthening of steel structures with high modulus carbon fibre reinforced polymer (CFRP) materials.” PhD Thesis, North Carolina State University, 265 pp.

Skaloud, M. and Zornerova, M. (2005). “The fatigue behaviour of the breathing webs of steel bridge girders.” Journal of Civil Engineering and Management, Vol. XI, No. 4, 323-336.

Yen, B. T. and Mueller, J. A. (1966) “Fatigue tests of large-size welded plate girders.” Welding Research Council, Bulletin No. 118, 1-25.

List of Tables:

List of Figures:

Table 1. Test variables in the final series of tests

Ref.	FRP type	Fibre orientation	Loading type	FRP panel alignment
SP-1	-	-	Static	-
SP-2	Glass	+45°/-45°	Static	Diagonal
SP-3	Carbon	0°/90°	Static	Diagonal
SP-4	Glass	+45°/-45°	Cyclic	Diagonal
SP-5	Carbon	0°/90°	Cyclic	Diagonal
SP-6	Carbon	0°/90°	Cyclic	45°

Table 2: Experimental test results

Ref.	Specimen	Panel alignment	Loading type	Cycle range, thousands	Loading range	Initial imperfection, mm	Ultimate load, kN	Ultimate residual load, kN
SP-1	Control	-	Static	-	-	2.76	87.9	-
SP-2	GFRP	Diagonal	Static	-	-	+0.35	113.7	-
SP-3	CFRP	Diagonal	Static	-	-	-1.47	105.2	-
SP-4	GFRP	Diagonal	Cyclic	0 - 500	35% - 70%	-0.38	-	128.04
				500 - 1000	40% - 80%			
SP-5	CFRP	Diagonal	Cyclic	0 - 1000	32% - 64%	+1.14	-	140.07
				1000 - 2000	38% - 76%			
SP-6	CFRP	45°	Cyclic	0 - 2000	37.5% -75%	+0.03	-	165.11

Table 3: Increase in stiffness and energy absorption for the strengthened specimens

Ref.	Specimen	Test method	Stiffness index	Energy absorption index
SP-1	Control Specimen	Static	1.0	1.0
SP-2	GFRP	Static	7.94	1.72
SP-3	CFRP	Static	-	-
SP-4	GFRP	Cyclic	-	-
SP-5	CFRP	Cyclic	3.74	2.02
SP-6	CFRP (45°)	Cyclic	9.36	2.46

Table 4: Enhancement in the fatigue life estimation of the strengthened specimens

Specimen	ΔL kN	$\Delta \varepsilon$ mm/mm	$\Delta \sigma_r$ MPa	$\Delta \gamma$ mm/mm	$\Delta \tau_r$ MPa	Eurocode fatigue equations	
						$N_{\sigma r}$	$N_{\tau r}$
Control	52.7	0.0011	220	0.0009	69.2	366,852	4,120,824
Life increase (times the control specimen)						1.0	1.0
SP-4	52.7	0.00072	143.7	0.0007	53.4	1,316,544	15,122,212
Life increase (times the control specimen)						3.56	3.67
SP-5	52.7	0.00074	147.9	0.00072	55.3	1,206,855	12,688,721
Life increase (times the control specimen)						3.29	3.08
SP-6	52.7	0.0007	140.9	0.0006	46.3	1,395,844	30,880,859
Life increase (times the control specimen)						3.80	7.49

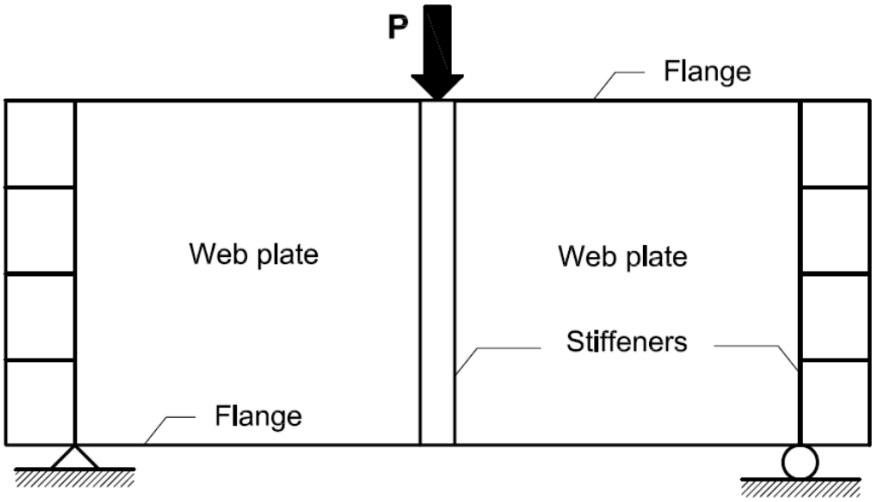

(**a**) Typical steel plate girder

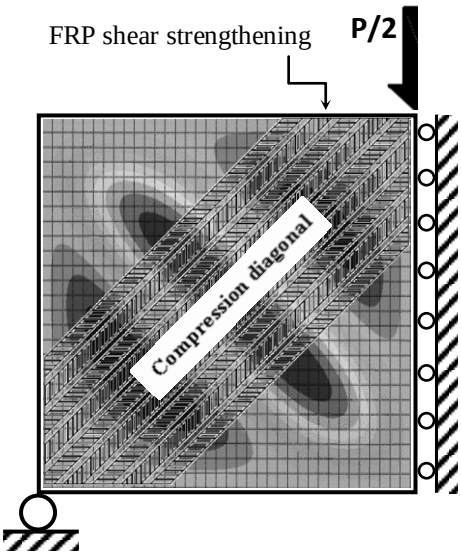

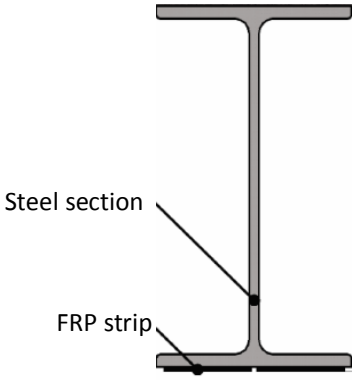

(**b**) Proposed FRP strengthening against shear buckling (**c**) FRP Flexural Strengthening

Fig. (1): Schematic showing the proposed strengthening technique compared to a typical flexural FRP strengthening.

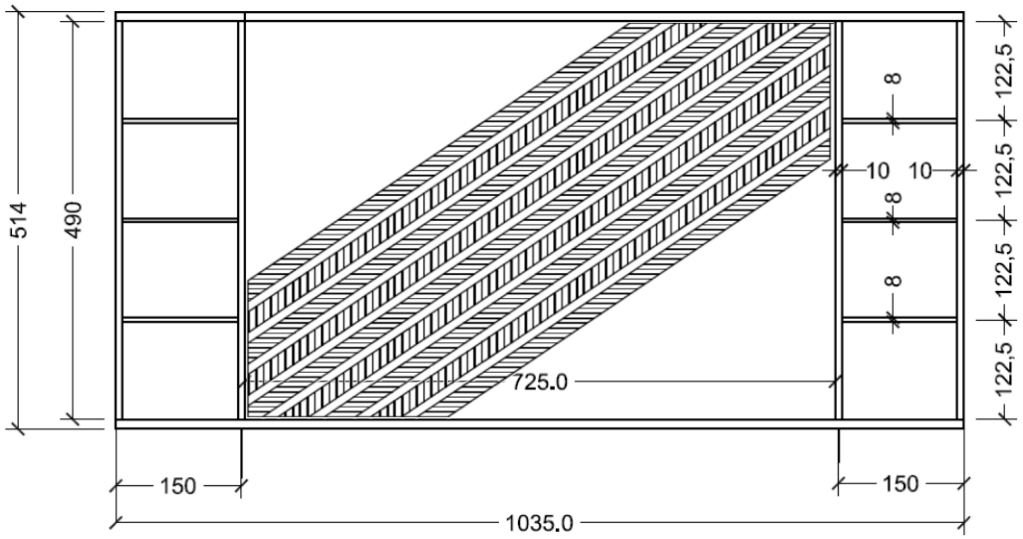

(**a**) Plate girder specimen details

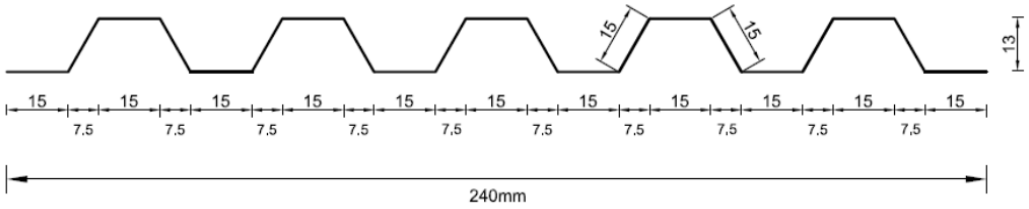

FRP section typically used for the first five specimens in the cyclic series of tests

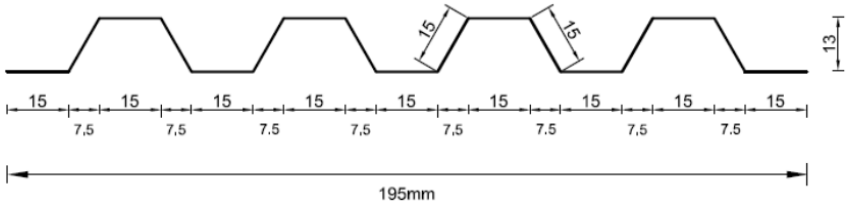

FRP section used for SP-6 in the cyclic series of tests

(**b**) FRP strengthening sections

Fig. (2): Specimen details and FRP sections

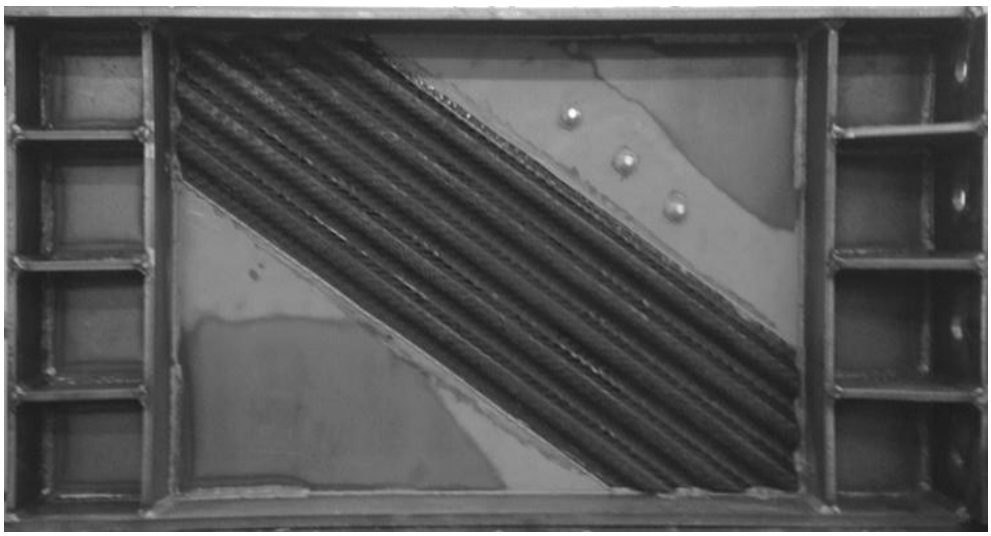

(**a**) SP-5 (CFRP- Diagonal)

(**b**) SP-6 (CFRP- 45°)

Fig. (3): Photos for the strengthened specimens.

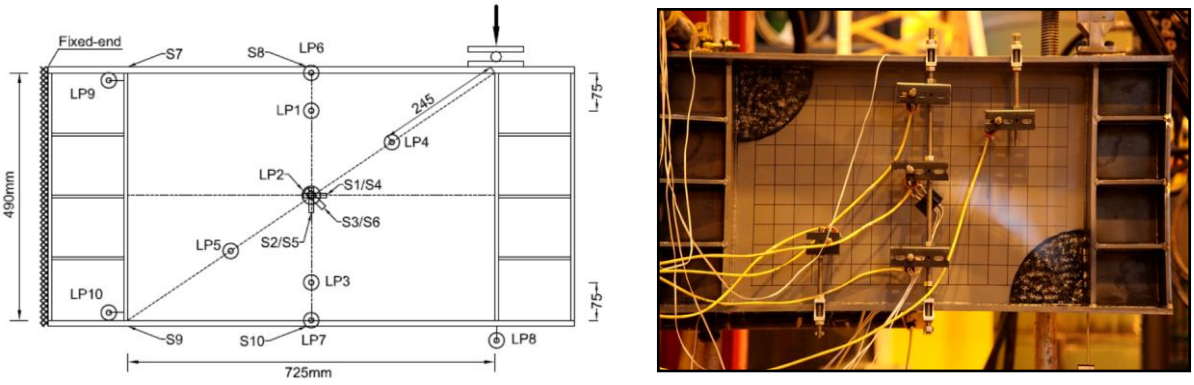

(**a**) SP-1 (Control specimen), SP-2 (GFRP), and SP-3 (CFRP) - Static tests

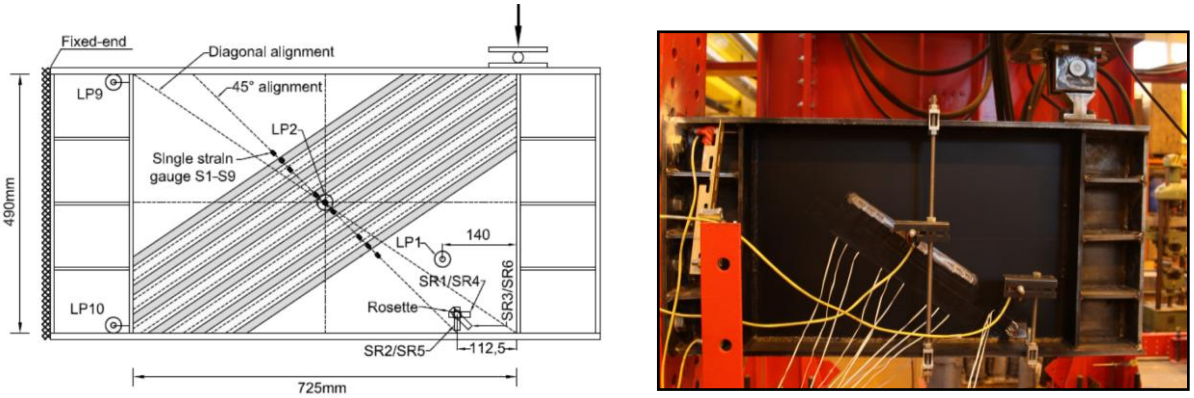

(**b**) SP-4 (GFRP) and SP-5 (CFRP) - Cyclic tests

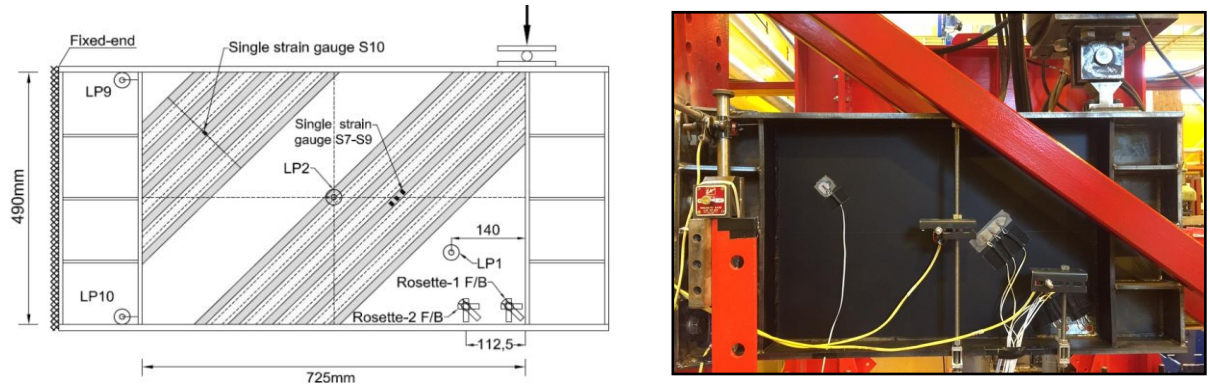

(**c**) SP-6 (CFRP) - Cyclic test

Fig. (4): Test instrumentation.

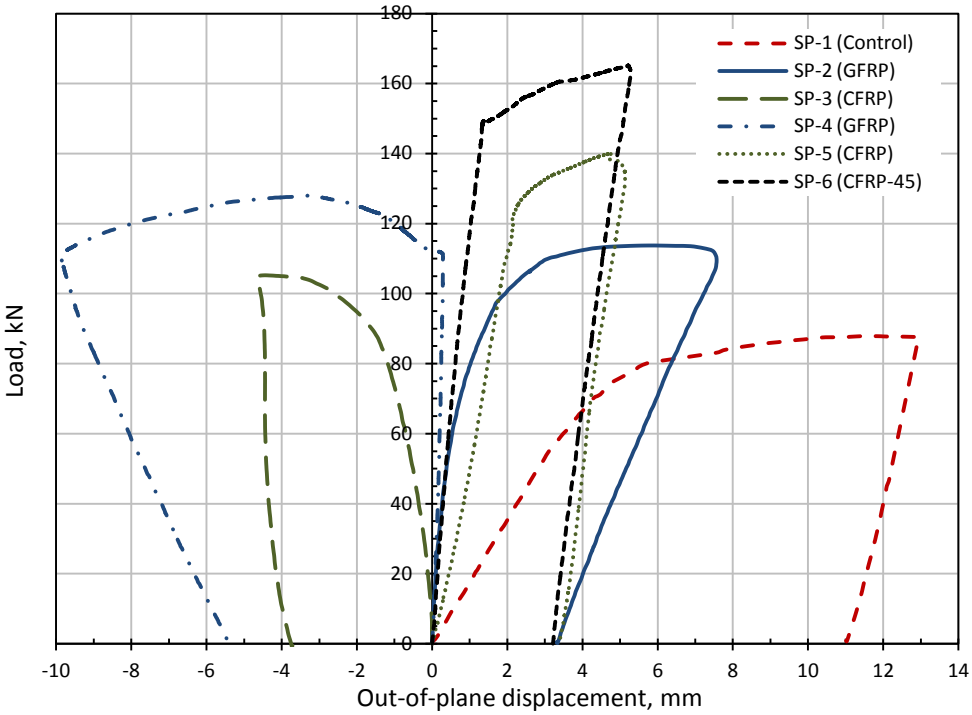

(**a**) Buckling curves

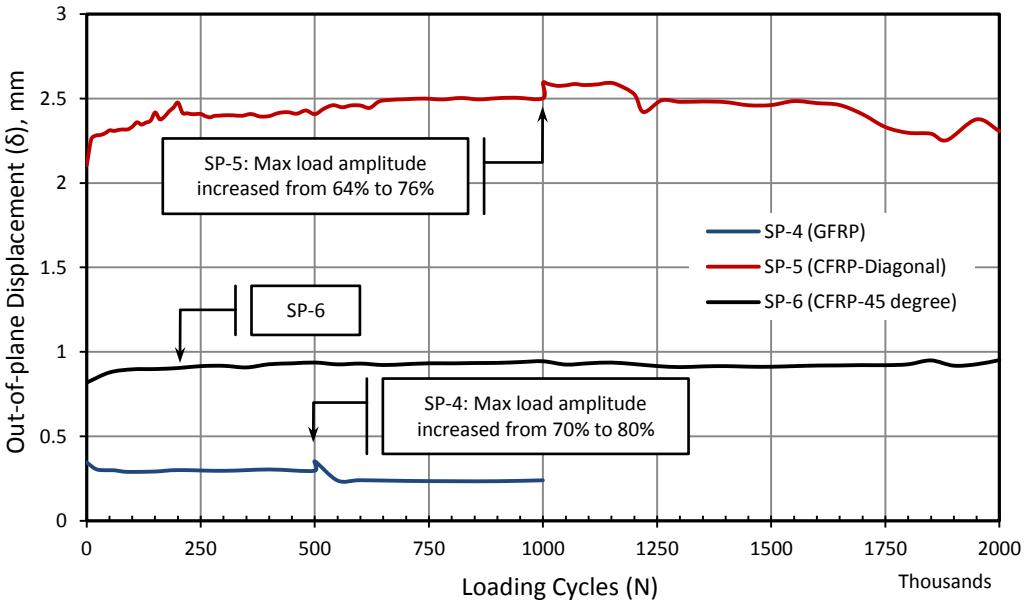

(**b**) Variations of the Out-of-plane displacement with the number of loading cycles

Fig. (5): Static and cyclic buckling curves for all tested specimens.

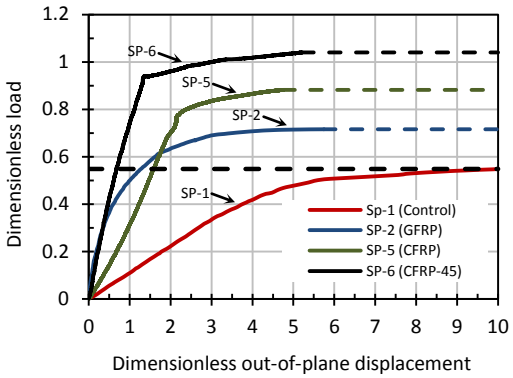

(**a**) Extended dimensionless buckling curves

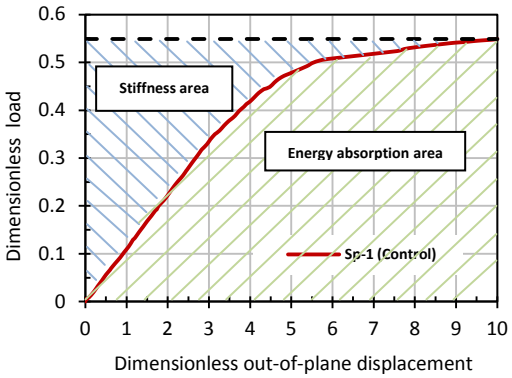

(**b**) Calculating the area under (energy absorption) and over (stiffness) the curve for the control specimen

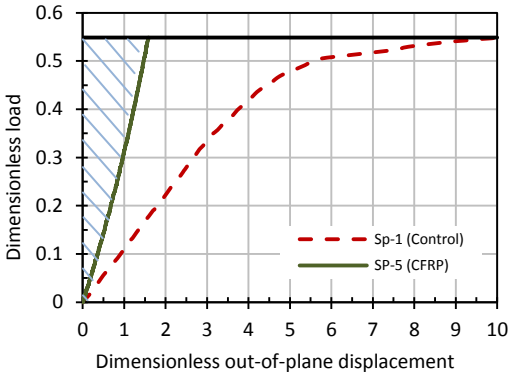

(**c**) An example for calculating the area over the curve (Stiffness) for SP-5

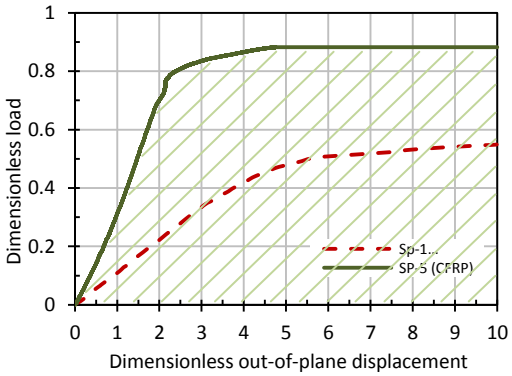

(**d**) An example for calculating the area under the curve (energy absorption) for SP-5

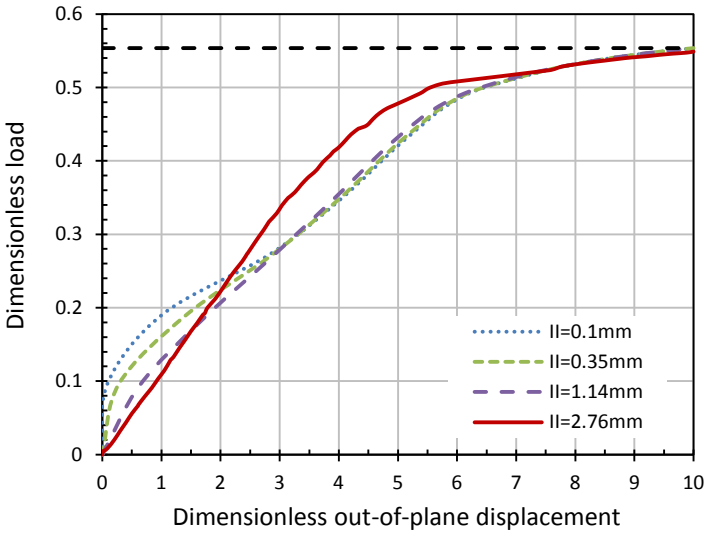

(**e**) Dimensionless buckling curves with different hypothetical initial imperfections analyzed using the FEM

Fig. (6): Assessing the stiffening effect of the proposed strengthening technique.

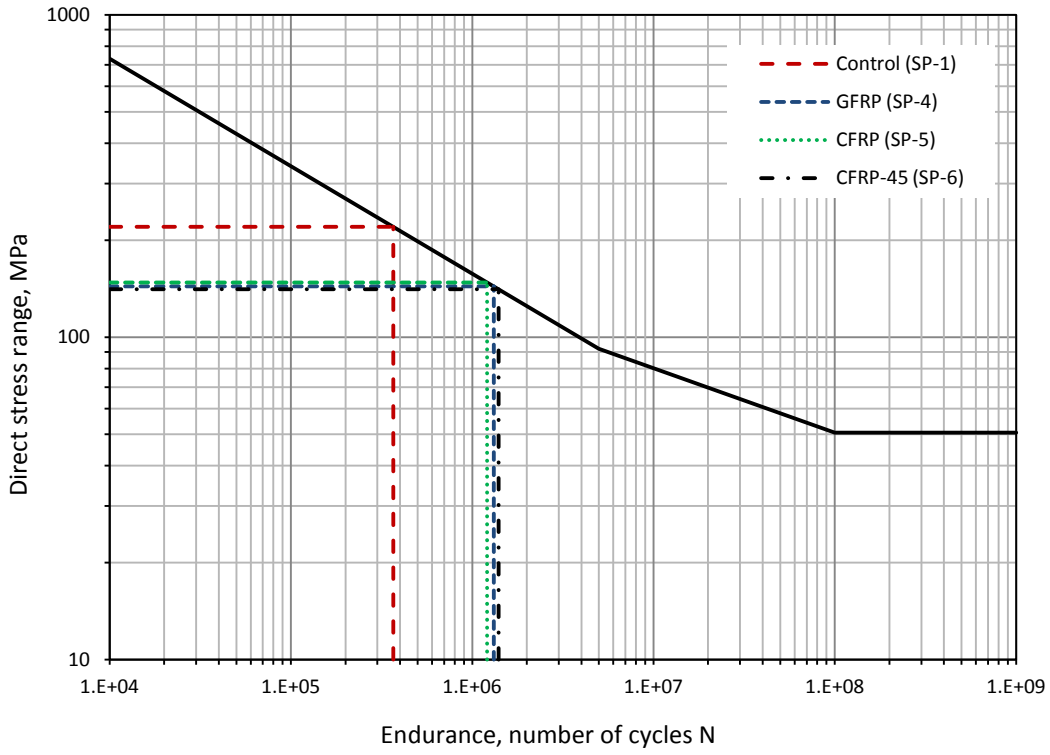

(**a**) Direct stress range – Detail category 125 N/mm^2

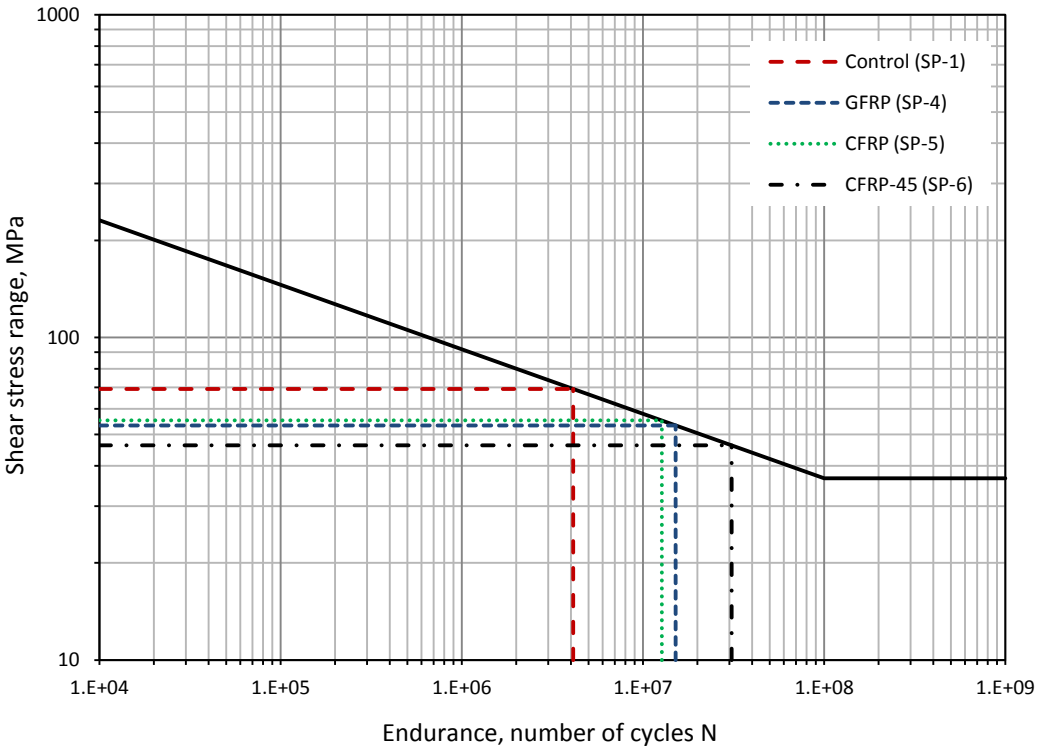

(**b**) Shear stress range - Detail category 80 N/mm^2

Fig. (7): Fatigue life estimation of the strengthened specimens.

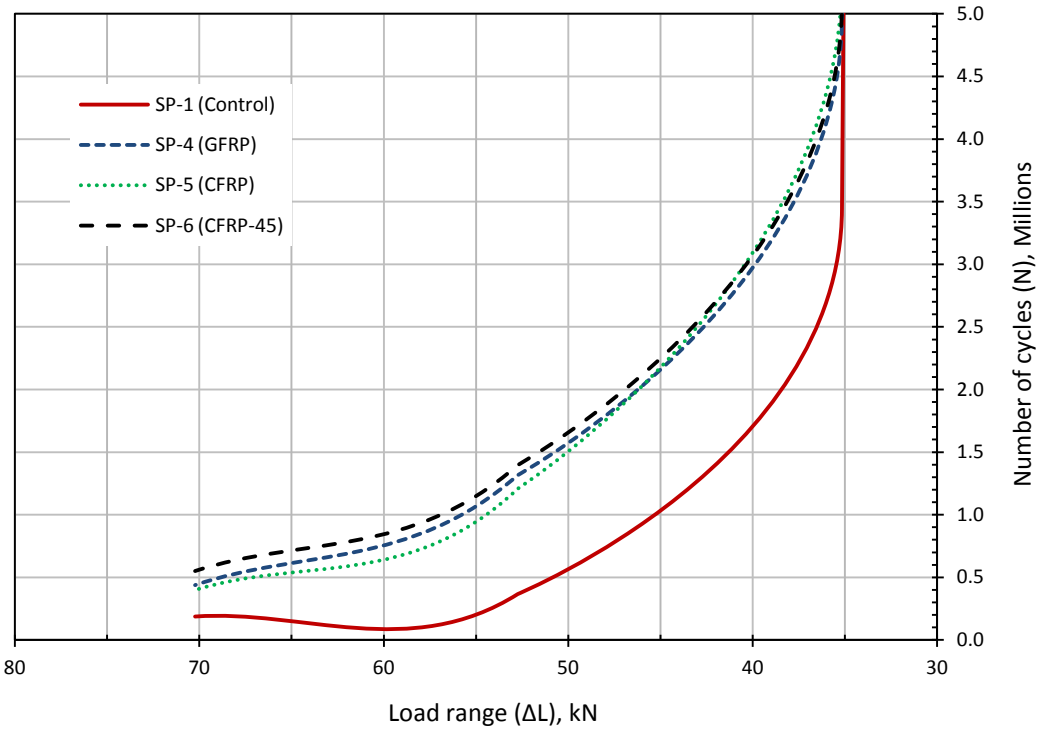

(**a**) Direct stress range criterion

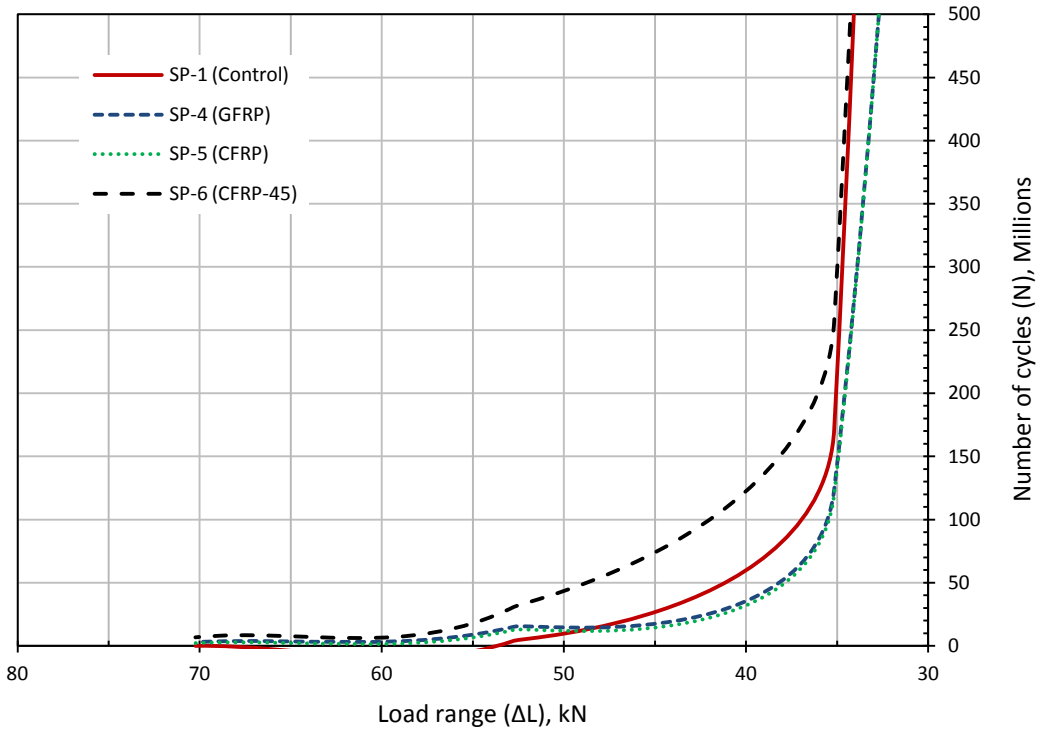

(**b**) Shear stress range criterion

Fig. (8): Fatigue life estimation of the strengthened specimens calculated with different load ranges.

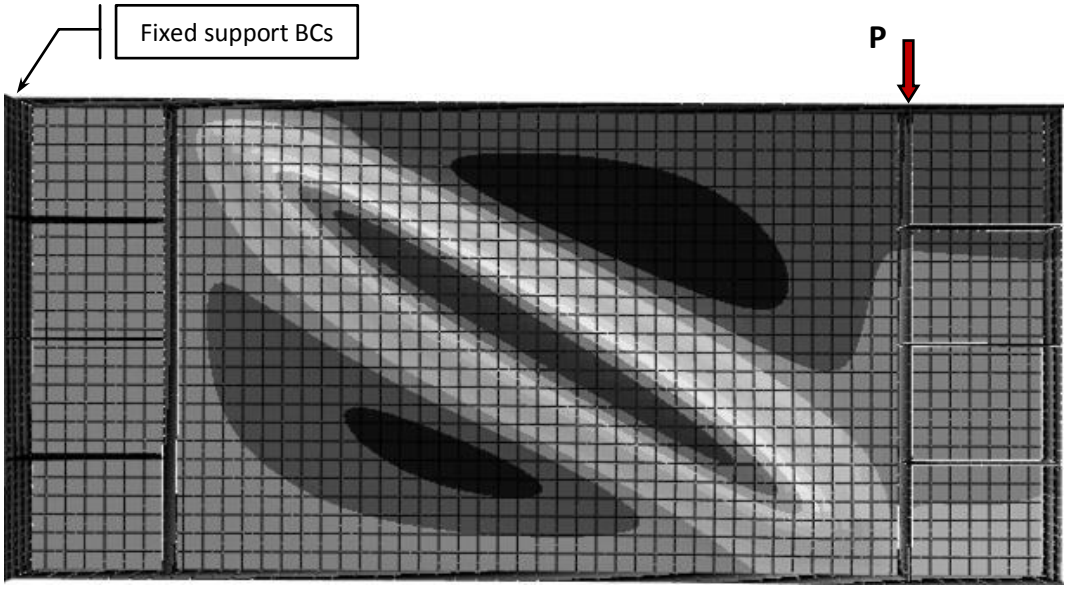

Fig. (9): Finite element model for the control specimen (SP-1).

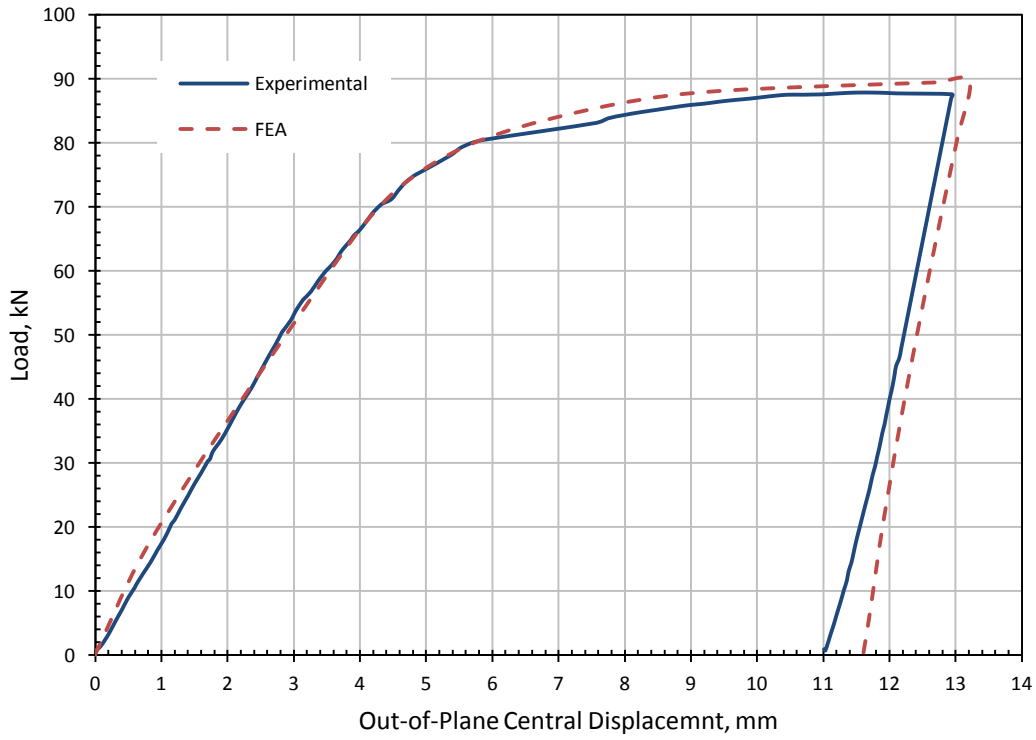

(**a**) Buckling curve of the control specimen (SP-1)

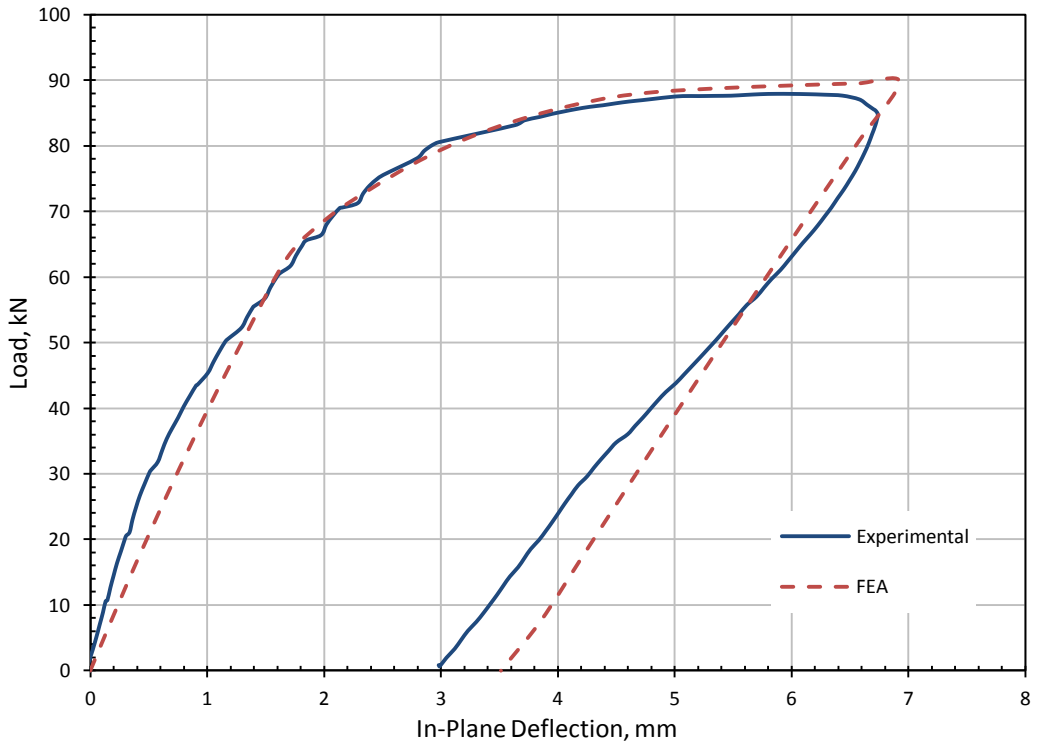

(**b**) Deflection curve of the control specimen (SP-1)

Fig. (10): Comparison between the experimentally measured deformations and the predictions of the finite element model.

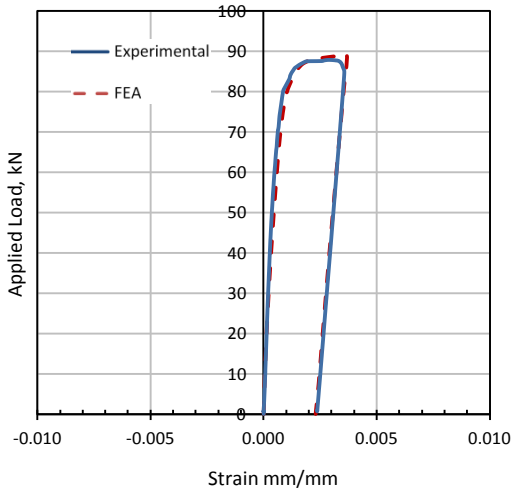

(**a**) ε_x front face

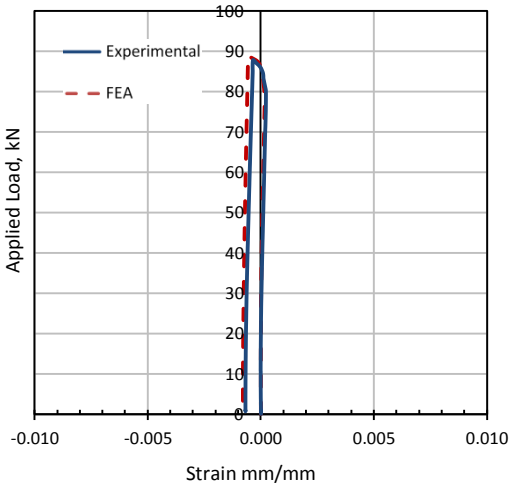

(**b**) ε_x back face

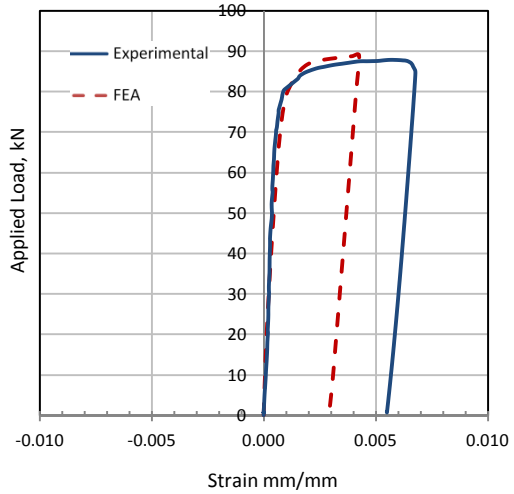

(**c**) ε_y front face

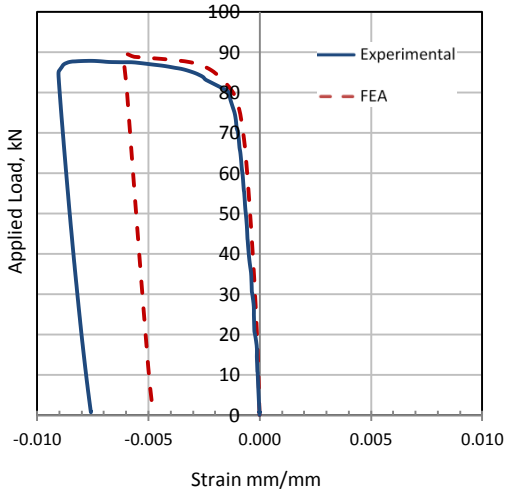

(**d**) ε_y back face

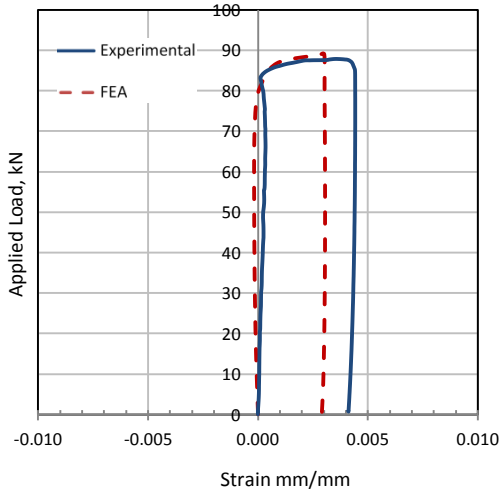

(**e**) Υ_{xy} front face

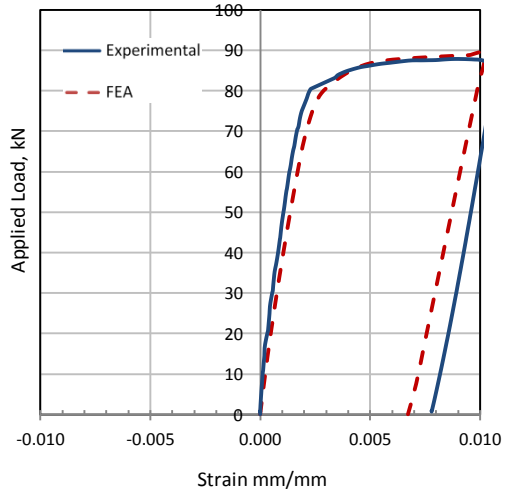

(**f**) Υ_{xy} back face

Fig. (11): Comparison between the experimentally measured strains and the predictions of the finite element model for the control specimen (SP-1).